Structural Studies of the Interaction between Ubiquitin Family Proteins and Proteasome Subunit S5a†

Kylie J. Walters,[‡,§,||] Maurits F. Kleijnen,[‡,§,⊥] Amanda M. Goh,[‡] Gerhard Wagner,[#] and Peter M. Howley*,[‡]

Department of Pathology and Department of Biological Chemistry and Molecular Pharmacology, Harvard Medical School, Boston, Massachusetts 02115

Received October 5, 2001; Revised Manuscript Received November 21, 2001

ABSTRACT: The 26S proteasome is essential for the proteolysis of proteins that have been covalently modified by the attachment of polyubiquitinated chains. Although the 20S core particle performs the degradation, the 19S regulatory cap complex is responsible for recognition of polyubiquitinated substrates. We have focused on how the S5a component of the 19S complex interacts with different ubiquitin-like (ubl) modules, to advance our understanding of how polyubiquitinated proteins are targeted to the proteasome. To achieve this, we have determined the solution structure of the ubl domain of hPLIC-2 and obtained a structural model of hHR23a by using NMR spectroscopy and homology modeling. We have also compared the S5a binding properties of ubiquitin, SUMO-1, and the ubl domains of hPLIC-2 and hHR23a and have identified the residues on their respective S5a contact surfaces. We provide evidence that the S5a-binding surface on the ubl domain of hPLIC-2 is required for its interaction with the proteasome. This study provides structural insights into protein recognition by the proteasome, and illustrates how the protein surface of a commonly utilized fold has highly evolved for various biological roles.

Regulated protein degradation is required for a variety of diverse cellular functions, including controlling the lifespan of regulatory proteins, removing misfolded proteins, and producing immunocompetent peptides (*1*−*6*). An important mechanism for controlled proteolysis is the ubiquitin-mediated pathway of proteasomal degradation. This pathway involves an enzymatic cascade that culminates in the covalent attachment of ubiquitin to protein substrates by E3 ubiquitin ligases (*7*−*9*). Polyubiquitin chains serve as general signals for protein degradation by the proteasome, and in vitro studies suggest that polyubiquitination of a substrate is sufficient for proteasome-mediated degradation (*2*).

The 26S proteasome is composed of two particles, a 19S regulatory complex and the 20S core particle (*1*, *10*). The 20S particle contains four stacked rings of seven subunits each that form a hollow cylinder, with catalytic sites situated on the interior surface. It provides the proteolytic activities, whereas the regulatory 19S cap complex confers ATP dependence and substrate recognition. The 19S complex comprises more than 30 subunits, which function to recognize and unfold target proteins that are to be degraded within the 20S core. The structure, assembly, and enzymatic mechanism of the 20S complex are well-characterized, whereas little is known of the functional organization of the 19S component. The research described here addresses the recognition of ubiquitin and ubiquitin family proteins by this component.

Polyubiquitin chains are recognized by the proteasome, and proteins that bear polyubiquitinated chains undergo proteasome-dependent degradation. The basis of the interactions between polyubiquitinated substrates and the proteasome remains an active area of investigation. One subunit of the 19S component, S5a, has been shown to bind polyubiquitin chains (*11*, *12*) as well as the ubiquitin-like domain of hHR23a and hHR23b, the human homologues of the yeast Rad23 protein (*13*). Although the structure of S5a has not yet been described, mutagenesis studies indicate that there are two independent polyubiquitin binding segments within S5a that are highly conserved among eukaryotes (*14*, *15*). Each segment contains five hydrophobic residues forming an alternating pattern of long and short side chains. The second ubiquitin-binding sequence of S5a, which is absent in yeast, is required for binding of hHR23a (*13*).

Mutations of the 26S protease subunits in yeast indicate that degradation of ubiquitinated substrates is essential for cell cycle progression (*16*, *17*). However, deletion of the *Saccharomyces cerevisiae* gene corresponding to S5a, *RPN10*, results in cells that are viable and in which the majority of short-lived proteins are degraded in a manner similar to that of wild-type cells (*18*, *19*). Since the polyubiquitinated substrates must be recognized by the proteasome, it follows that Rpn10 may not be the only proteasome subunit responsible for polyubiquitin chain recognition in yeast. The steady-state levels of polyubiquitin conjugates in ΔRPN10 yeast cells do increase in vivo, indicating that Rpn10 does however contribute to the in vivo degradation of polyubiq-

† This work was supported by grants from the National Institutes of Health (GM47467 to G.W. and R37-CA64888 to P.M.H.). K.J.W. was supported in part by a grant from Aid For Cancer Research (Boston, MA) and by a grant from the American Cancer Society.

* To whom correspondence should be addressed. Telephone: (617) 432-2884. Fax: (617) 432-2882. E-mail: peter_howley@hms.harvard.edu.

‡ Department of Pathology.

§ These authors contributed equally to this work.

|| Present address: Department of Biochemistry, Molecular Biology, and Biophysics, University of Minnesota, Minneapolis, MN 55455.

⊥ Present address: Department of Cell Biology, Harvard Medical School, Boston, MA 02115.

Department of Biological Chemistry and Molecular Pharmacology.

10.1021/bi011892y CCC: $22.00
Published on Web 01/18/2002

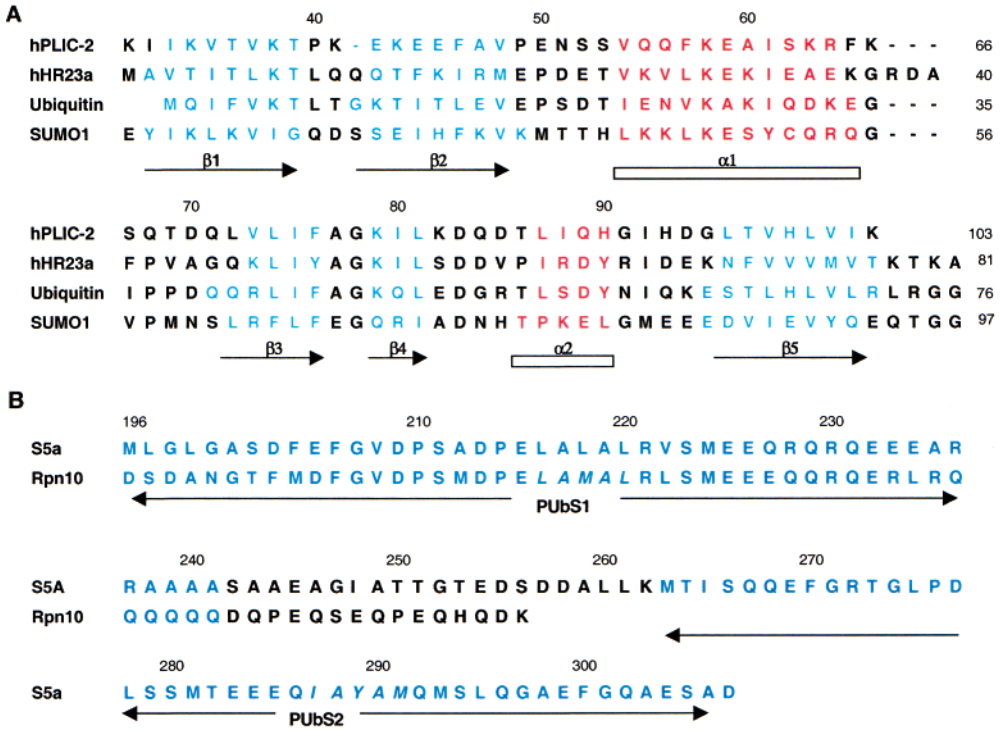

FIGURE 1: Sequence alignment of the hPLIC-2 ubl domain, the hHR23a ubl domain, ubiquitin, and SUMO-1. This alignment was based on the reported (for ubiquitin and SUMO-1) (*40*, *41*) and determined (for the ubl domains of hPLIC-2 and hHR23a) secondary structural elements. Secondary structural elements are displayed below the sequence, and residues involved in β-strands and helices are colored blue and red, respectively.

uitin conjugates in yeast (*18*). Interestingly, a yeast strain lacking both *RAD23* and *RPN10* has a delay in the G2−M transition of the cell cycle and increased levels of multiubiquitinated proteins (*20*).

Ubiquitin is homologous with two families of ubiquitin-like proteins (*21*). Like ubiquitin, type 1 ubiquitin-like (ubl)[1] proteins, such as SUMO and Nedd8, are cleaved at a diglycine motif and are covalently attached to other proteins through their C-terminal glycine. Proteins covalently modified by these type 1 ubl proteins are not targeted to the proteasome for degradation, but are associated with a variety of cellular functions (*22*). Type 2 ubl domains exist in the N-terminal region of multidomain proteins, and although these proteins have been actively studied and associated with important cellular processes, their biological functions are unclear. We present here descriptions of how two of these proteins interact with the proteasome via their type 2 ubl domains.

We have focused our study on hHR23a and hPLIC-2, the human homologues of Rad23 and Dsk-2, respectively. Rad23 plays an important role in the nucleotide excision repair (NER) pathway and has been implicated in spindle pole body duplication and cell cycle progression in *S. cerevisiae* (*23*−*25*). Dsk-2 has been implicated in spindle pole body duplication (*23*). The mammalian homologues of Rad23 (hHR23a and hHR23b) also function in NER (*26*), whereas the mammalian homologues of Dsk-2 (PLIC-1 and PLIC-2) have only recently been described (*27*, *28*). In our laboratory, hHR23a and hPLIC-2 were identified in a yeast two-hybrid screen as interactors of the E3 ubiquitin ligase E6AP (*28*, *29*). Each of these proteins has also been shown to interact with the proteasome (*13*, *28*). The different roles of these domains and their significance for proteasome targeting however are not known. The sequence alignment of the ubiquitin-like domains of hPLIC-2, hHR23a, and SUMO-1 compared to ubiquitin is shown in Figure 1. As discussed below, this sequence alignment is based on superimposing the experimentally determined secondary structural elements.

In this work, we provide structural insights into the different binding properties of the ubiquitin family proteins with the proteasome and characterize the proteasome-binding surfaces on members of this family. We have used nuclear magnetic resonance (NMR) spectroscopy to determine the structure of the ubl domain of hPLIC-2 and have found that this structure more closely resembles ubiquitin than the type 1 ubiquitin-like protein SUMO-1. Furthermore, we have determined the secondary structure of the hHR23a ubl domain by NMR spectroscopy. We have used this information to build a homology-based model of the hHR23a ubl domain based on our calculated structure of the ubl domain of hPLIC-2. We then identified the residues of ubl domains of hPLIC-2 and hHR23a, and of ubiquitin, that serve to contact S5a. Our results indicate that there is an S5a-binding surface conserved between the type 2 ubl domains of hPLIC-2 and hHR23a. The analogous surface in ubiquitin differs slightly from that of the type 2 ubl domains, and these differences provide an explanation for an observed weaker binding of ubiquitin to S5a. The S5a-binding region on the surface of the hPLIC-2 ubl domain was verified by creating specific amino acid substitutions within the identified binding surface that were able to disrupt binding between the two

[1] Abbreviations: 1D, one-dimensional; 2D, two-dimensional; 3D, three-dimensional; hPLIC, human proteasome ligase interaction component; HSQC, heteronuclear single-quantum coherence; NER, nucleotide excision repair; NMR, nuclear magnetic resonance; NOE, nuclear Overhauser effect; ubl, ubiquitin-like.

proteins. The same substitutions also abrogated all binding of the hPLIC-2 ubl domain to the proteasome, indicating that this surface on the ubl domain is required for binding to intact proteasomes. Furthermore, we found that the type 1 ubl protein, SUMO-1, in which the electrostatic properties of this surface are not conserved, does not bind S5a.

Comparisons of the type 2 ubl domains with SUMO-1 and ubiquitin reveal how this conserved protein fold may be used for very different biological functions through changes in the electrostatic potential at the protein surface. Our studies reveal the surface within the ubl domains of hPLIC-2 and hHR23a that is necessary for proteasome binding. Furthermore, on the basis of our structure comparison with ubiquitin, we provide an explanation for why ubiquitin is a weaker S5a binding protein than hPLIC-2 and hHR23a. Our study indicates why some ubiquitin family proteins target the proteasome whereas others do not.

MATERIALS AND METHODS

Sample Preparation. All the proteins in this study were produced from pET vectors (Novagen) containing an in-frame C-terminal histidine tag. The plasmids containing these genes were each transformed into BL21(DE3) cells and grown at 37 °C in M9 minimal medium or in Luria broth containing ampicillin (100 μg/mL). Protein expression was induced by adding IPTG, once absorption at 600 nm surpassed 0.4. The cells were then grown at 25 °C for an additional 12 h. After being harvested by centrifugation (5000*g* for 20 min), the cells were lysed by sonication and then centrifuged again at 15000*g* for 30 min. The supernatant was then applied to 1 mL of nickel−NTA agarose beads (Qiagen) per liter of cells and, after extensive washing, eluted with 0.25 M imidazole. Lysis and washing were performed in 300 mM NaCl and 50 mM $NaPO_4$ (pH 6.0). Gel filtration with an FPLC-Superdex-75 column (Pharmacia) was subsequently performed on all samples, except S5a, in 100 mM NaCl and 50 mM $NaPO_4$ (pH 6.5). Labeled samples were prepared by using [^{13}C]glucose and $^{15}NH_4Cl$ as the sole carbon and nitrogen source, respectively (Cambridge Isotopes). NMR experiments were typically carried out at 25 °C with 1.0 mM samples in 50 mM sodium phosphate buffer (pH 6.5), 100 mM NaCl, and 0.1% sodium azide. Point mutations were generated by site-directed mutagenesis (QuikChange, Stratagene) and confirmed by DNA sequencing.

NMR Spectroscopy. All spectra were acquired at 600 MHz (Bruker DMX) or 500 MHz (Bruker DMX with a cryoprobe, Varian Unity or Varian INOVA). Resonance assignments were obtained for the ^{15}N, Cα, and ^{N}H atoms of the ubl domains of hPLIC-2 and hHR23a by using standard 3D heteronuclear [^{1}H,^{15}N,^{13}C]HNCA and HN(CO)CA experiments (*30*). By using these experiments, we were able to sequentially align spin systems via their Cα atoms. The chemical shift values of the Cα atoms were used to reveal the secondary structural elements of the ubl domain of hHR23a and hPLIC-2 (*31*, *32*). Distance restraints for the ubl domain of hPLIC-2 were obtained by using ^{15}N-dispersed (120 ms mixing time), ^{13}C-dispersed (80 ms mixing time), and 2D (80 and 120 ms mixing times) NOESY spectra. The ^{13}C-dispersed NOESY and the 2D homonuclear NOESYspectra with a mixing time of 80 ms were recorded in D_2O. Distance restraints for the ubl domain of hHR23a were obtained by using a ^{15}N-dispersed NOESY spectrum with a mixing time of 120 ms. The pattern of NOE interactions for each amino acid was used to reveal the secondary structure and hydrogen bonding of both proteins (*33*). Spectra were processed with FELIX software packages (Hare Research, Inc./Biosym Inc.) and analyzed by using XEASY (*34*) on a Silicon Graphics workstation. Dihedral ϕ and ψ angles were obtained with the TALOS program (*35*). Furthermore, from geometric considerations, when the NOE from the proceeding α-proton to an amide proton was stronger than the intraresidue NOE, the backbone dihedral ϕ angle of that residue was set to -20 to $-180°$.

Table 1: Structural Statistics for NMR Structure Calculations Performed in XPLOR Version 3.851

total no. of NOE distance restraints	1068
inter-residue	680
medium-range	162
$i, i+2$	75
$i, i+3$	57
$i, i+4$	30
long-range ($\|i-j\| > 4$)	239
no. of hydrogen bonds	23
dihedral angle restraints (deg)	
ϕ [$C'_{(i-1)}$−N_i−Cα_i−C'_i]	23
φ (N_i−Cα_i−C'_i−N_{i+1})	21
Ramachandran plot (%)	
most favorable region	72.9
additionally allowed region	21.0
generously allowed region	5.9
disallowed region	0.2
av rmsd for distance restraints (Å)	$1.65 \times 10^{-2} \pm 1.2 \times 10^{-3}$
av rmsd for dihedral restraints (deg)	$(0.81 \pm 7.2) \times 10^{-2}$
av rmsd from idealized covalent geometry	
bonds (Å)	$2.0 \times 10^{-3} \pm 6.2 \times 10^{-5}$
angles (deg)	$(0.55 \pm 4.9) \times 10^{-3}$
improper angles	$(0.41 \pm 1.1) \times 10^{-2}$
av rmsd of backbone atoms from the average structure within regions of secondary structure (Å)	$(0.41 \pm 7.2) \times 10^{-2}$
av rmsd of all heavy atoms from the average structure within regions of secondary structure (Å)	$(0.97 \pm 7.7) \times 10^{-2}$

Structure Calculations. Structure calculations were performed, based on the NOE distance and dihedral angle restraints described in Table 1, with the use of simulated annealing (*36*) in XPLOR version 3.851 (*37*) on a R12000 Octane Silicon Graphics workstation. A total of 20 random structures were subjected to 60 000 simulated annealing and cooling steps of 0.005 ps. Coordinate and restraint files have been submitted to the Protein Data Bank (PDB entry 1J8C).

NMR Spectroscopy Experiments for S5a Binding. To characterize the interaction with S5a, a NMR titration study was performed where the [^{15}N,^{1}H]HSQC spectrum of each ubiquitin-like domain was monitored upon addition of increasing concentrations of S5a. Concentrations were calculated by using extinction coefficients based on amino acid composition. The absorbance at 280 nm was measured for each protein in urea, and the concentration of the ubl domains, ubiquitin, and SUMO-1 used in the [^{1}H,^{15}N]HSQC experiments was 0.3 mM. In these binding titration experiments, we measured the change in the chemical shift of the amide nitrogen and proton atoms of [^{1}H,^{15}N]HSQC cross-peaks of the ^{15}N-labeled protein according to the equation $\sqrt{(0.2\delta_N^2) + \delta_H^2}$, where δ_N and δ_H represent the change in

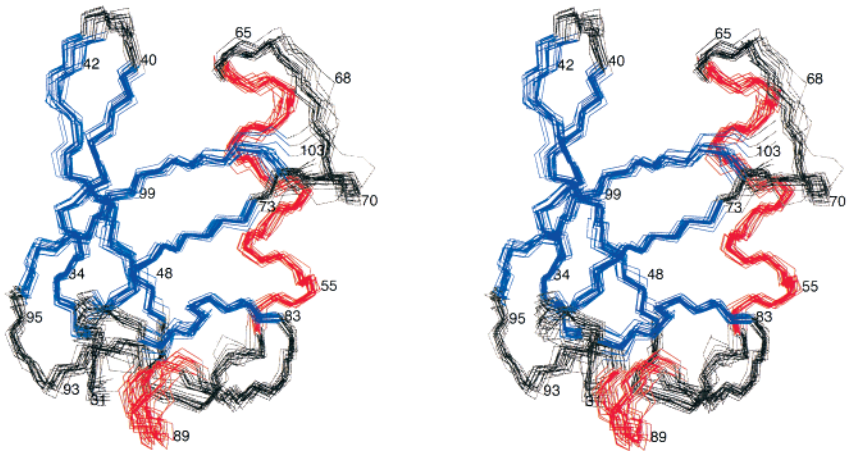

FIGURE 2: Stereoview of superimposed structures of the ubl domain of hPLIC-2. The backbone atoms of residues in regions of regular secondary structure are superimposed, and those residues involved in β-strands and helices are colored blue and red, respectively. This figure was produced using the program MOLMOL (*50*).

nitrogen and proton chemical shifts upon S5a addition, respectively.

In Vitro Binding Experiments. Bacterial pellets from 500 mL OF IPTG-induced (0.5 mM, 25 °C overnight) cultures containing wild-type or 75/77/99 mutant hPLIC-2 ubl-His tag pET (Novagen) fusion constructs or a control plasmid were resuspended in PBS (8 mL/pellet) and sonicated. Lysates were cleared by centrifugation (10000*g* for 20 min) and incubated with 250 μL of PBS-washed nickel−NTA agarose beads (Qiagen) for 1.5 h at 4 °C to achieve high concentrations of the ubl proteins on the beads. After being washed in PBS, the bound proteins on the beads were analyzed by SDS−PAGE and Coomassie staining. Two 150 cm^2 subconfluent dishes of HeLa cells were harvested in 4 mL of NP-40 lysis buffer [50 mM Tris (pH 8), 0.5% NP-40, and 5 mM $MgCl_2$], and lysates were cleared by centrifugation and split into four fractions, each of which was incubated for 1.5 h at 4 °C with 20 μL of nickel−NTA beads loaded with the different ubl proteins. The beads were washed in the same lysis buffer, subjected to SDS−PAGE, and transferred to a membrane for Western blot analysis using the α-2 proteasomal core subunit (α-p25 is clone 7A11, ICN/Cappel).

RESULTS

Structure Determination of the Ubl Domain of hPLIC-2 and Comparisons with Ubiquitin and SUMO-1. The human PLIC-2 protein contains 624 amino acids with a ubiquitin-like domain in the N-terminal region, as well as collagen-like and ubiquitin-associated domains in the C-terminal region (*28*). We analyzed by NMR spectroscopy a fragment of PLIC-2 consisting of residues 1−104, including the ubiquitin-like domain (containing amino acids 31−103). For ease of purification, we prepared a construct in which the C-terminal region contains a linker region of 16 amino acids attached to a six-residue histidine tag.

The structure of the ubl domain of hPLIC-2 was determined by previously described procedures (*38*). A summary of the NMR data used for structure calculations is provided in Table 1. Structure calculations were performed with the use of simulated annealing (*36*) in XPLOR version 3.851 (*37*) on a R12000 Octane Silicon Graphics workstation. All 20 random starting structures converged with no NOE or dihedral angle violation greater than 0.3 Å or 5°, respectively. The average root-mean-square deviations from the average structure within the secondary structural elements of residues 33−101 (including residues 33−39, 42−48, 53−62, 73−76, 79−82, 87−90, and 96−101) for the backbone atoms and for all heavy atoms are 0.41 and 0.97 Å, respectively. A stereoview of the 20 calculated structures superimposed is provided in Figure 2. Although the N-terminal hPLIC-2 fragment used in this study contains the first 30 residues preceding the ubl domain, these residues are omitted in all figures because they are disordered in this construct. The C-terminal region containing the linker and histidine tag were also found to lack NOE interactions, and the chemical shift frequencies of these residues were characteristic of a random coil structure.

The backbone structure of the hPLIC-2 ubl domain more closely resembles ubiquitin (*39*, *40*) than SUMO-1 (*41*) as displayed in Figure 3A. The root-mean-square deviation from the ubl domain of hPLIC-2 for the backbone atoms of residues situated in helices or β-strands is 2.0 Å for ubiquitin and 2.8 Å for SUMO-1. Comparisons of the positions and lengths of the secondary structural elements of all three proteins are included in Figure 1A. All three proteins contain five β-strands, an α-helix of 3.5 turns, and an additional 3_{10}-helix. In all three proteins, the first and last β-strands (β1 and β5, respectively) are oriented parallel to each other and all other neighboring β-strands are oriented antiparallel to each other. The orientation of β3 and β5 relative to α1 of the type 2 ubl domain of hPLIC-2 is more similar to that of ubiquitin than to that of SUMO-1. Although the fold of these three proteins is similar, their electrostatic surface potentials differ greatly. Figure 3 displays the electrostatic potential mapped onto a surface diagram for the ubl domain of hPLIC-2 (panel B), ubiquitin (panel C), and SUMO-1 (panel D). The orientation displayed on the left in panels B−D of Figure 3 is identical to that in Figures 2 and 3A, whereas that on the right is rotated by 180°. Basic, acidic, and hydrophobic regions are shown in blue, red, and white, respectively. In the orientation on the left, SUMO-1 is dramatically more acidic than ubiquitin and the ubl domain of hPLIC-2. As discussed below, this face is implicated in binding S5a.

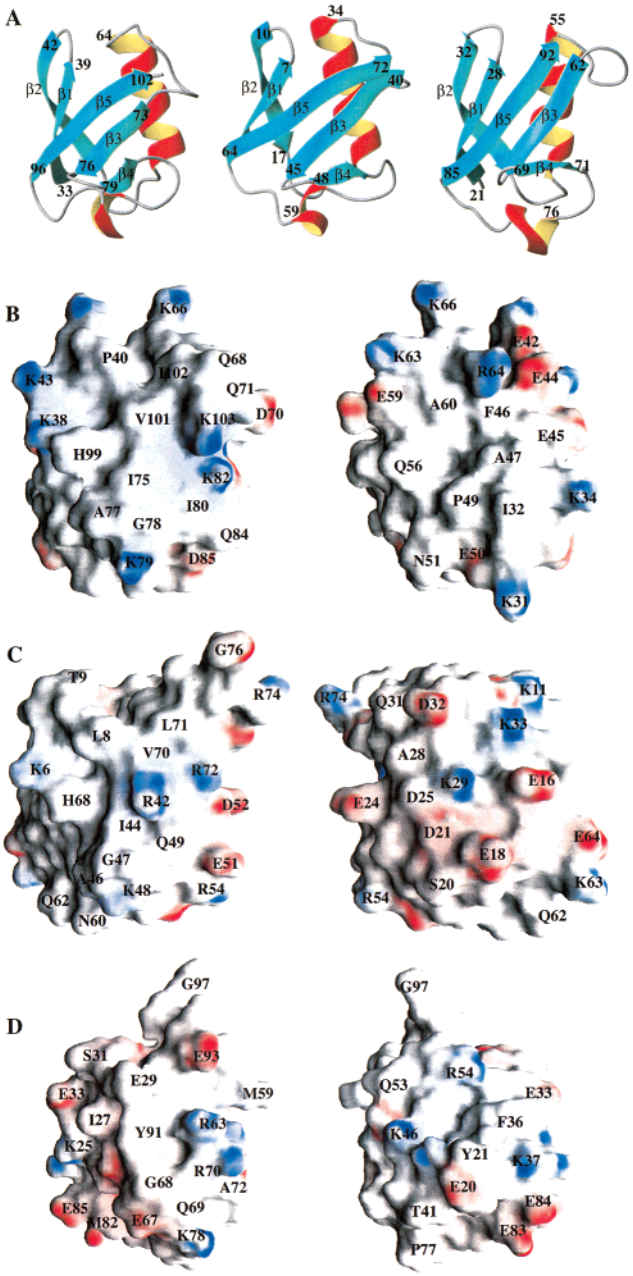

FIGURE 3: Comparison of the fold and electrostatic surface potential of the hPLIC-2 ubl domain, ubiquitin, and SUMO-1. Panel A contains ribbon diagrams of the backbone atoms of the ubl domain of hPLIC-2 (left), ubiquitin (middle), and SUMO-1 (right). The electrostatic surface potential is mapped onto the surface diagrams of the hPLIC-2 ubl domain (B), ubiquitin (C), and SUMO-1 (D). The orientation of the figures on the left in panels B−D is identical to that presented in panel A, whereas that on the right is rotated by 180°. The parameters used to generate each of these surface potentials are −42 to −21 and 42−21 kT. Panel A was produced with MOLMOL (*50*), and panels B−D were generated with GRASP (*51*).

The Ubl Domain of hPLIC-2 Binds the S5a Proteasome Subunit with a Hydrophobic Surface. Comparison of the [^{1}H,^{15}N]HSQC spectra of ^{15}N-labeled ubl domains of hPLIC-2 or hHR23a alone and with a 1:1 ubl:S5a molar ratio reveals binding of these type 2 ubl domains with S5a (Figure 4A,B). The disappearance of the signal originates from resonance broadening due to the increased rotational correlation time of the complex. This increased rotational correlation time is caused by the increased molecular mass of the complex. In the case of the hPLIC-2 ubl domain, for example, the molecular mass is increased from 14 kDa in the free form to 55 kDa in the complex with S5a. The strong resonances that remain in the [^{1}H,^{15}N]HSQC spectrum on the right of the ^{15}N-labeled hPLIC-2 ubl domain originate from either the first 30 residues N-terminal to the ubl domain or the last 22 residues, including a linker region and the histidine tag. These residues were all found to be structurally disordered in the ubl domain alone and in the complex of the ubl domains with S5a.

In addition to the apparent resonance broadening of residues within the ubl domain of hPLIC-2, a detailed comparison of the [^{1}H,^{15}N]HSQC spectra revealed that some resonances from these residues experienced chemical shift changes in the presence of S5a. Such chemical shift changes are caused by changes in the chemical environment of those atoms and, provided that there are no gross structural changes, can be used to map contact surfaces (*42*). By measuring the change in the chemical shift of the amide nitrogen and proton atoms in [^{1}H,^{15}N]HSQC spectra of the ^{15}N-labeled ubl domain in the absence and presence of increasing quantities of S5a, we were able to map the S5a interaction surfaces. At an equimolar concentration with S5a, all of the cross-peaks could be observed in 1D traces along the nitrogen and proton dimensions. By comparing the 1D traces in both dimensions of [^{1}H,^{15}N]HSQC spectra acquired in the absence and at an equimolar concentration of S5a, we were able to measure the change in the amide nitrogen and proton chemical shift.

Figure 5A displays the measured chemical shift changes of the amide nitrogen and hydrogen atoms of each residue according to eq 1

$$\sqrt{(0.2\delta_N{}^2) + \delta_H{}^2} \qquad (1)$$

where δ_N and δ_H represent the change in nitrogen and proton chemical shifts (in parts per million), respectively, upon S5a addition. The values presented in Figure 5A are then mapped onto the surface diagram of the ubl domain of hPLIC-2 in Figure 6A. In this figure, residues experiencing the greatest perturbation in their amide nitrogen and proton chemical shifts are colored most blue, whereas those residues not experiencing changes in the resonance frequencies of their amide nitrogen and proton atoms are white. Figure 6A is displayed in the same orientation as that of Figure 3, and those residues, including proline, whose chemical shift perturbation could not be measured are red. The S5a contact surface revealed by this technique is localized to a hydrophobic surface of the hPLIC-2 ubl domain and predominately involves residues located in the third, fourth, and fifth β-strands.

The hHR23a Ubl Domain Binds S5a with a Surface Almost Identical to the S5a-Binding Surface of the hPLIC-2 Ubl Domain. To determine whether a similar interaction surface in hHR23a contacts the proteasome, we assigned the Cα, N, and ^{N}H atoms of the ubl domain of hHR23a by using triple-resonance experiments. We located regions of regular secondary structural elements based on the chemical shift index of the Cα atoms, in combination with observed amide−amide NOE interactions in a ^{15}N-dispersed NOESY spectrum (*33*). The amide−amide NOE data also contained information about the hydrogen bonding patterns between

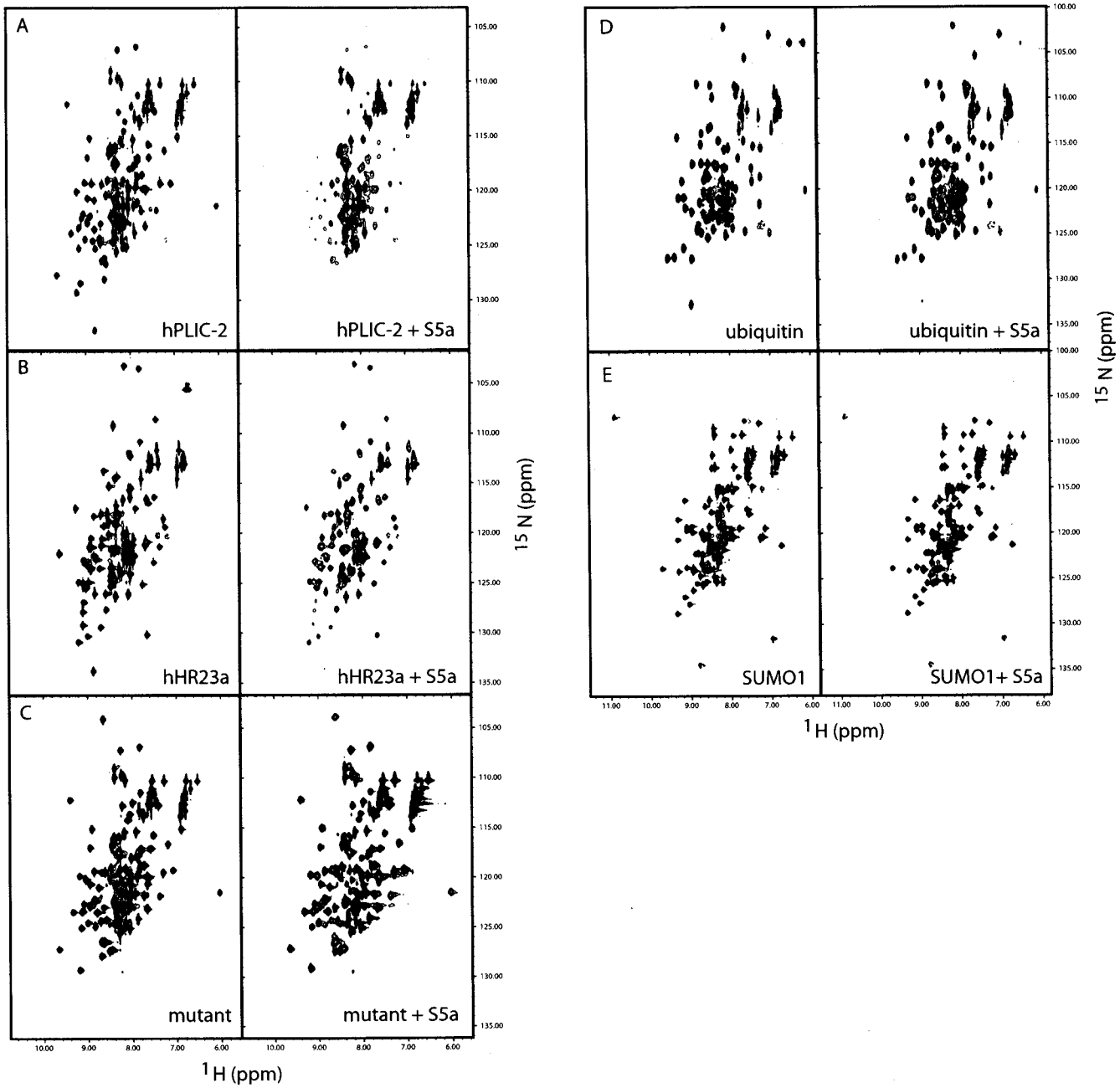

FIGURE 4: [^{1}H,^{15}N]HSQC spectra of the hPLIC-2 ubl domain (A), the hHR23a ubl domain (B), the hPLIC-2 triple mutant (I75A/A77S/H99A) ubl domain (C), ubiquitin (D), and SUMO-1 (E) alone (left) and with a 1:1 molar ratio with unlabeled S5a (right). We provide an enlarged view of a portion of these spectra as Supporting Information. Furthermore, in all cases, titrations were continued to a >1:2 molar ratio with S5a.

β-strands. Using this knowledge of the secondary structure of hHR23a and of hydrogen bonds between certain β-strands, we generated a model structure of the hHR23a ubl domain based on the calculated hPLIC-2 ubl domain structure, by using Look version 3.5.2 (*43*).

The [^{1}H,^{15}N]HSQC spectra of the ^{15}N-labeled hHR23a ubl domain alone and with a 1:1 hHR23a ubl domain:S5a molar ratio are displayed in Figure 4B on the left and right, respectively. As in the case with the hPLIC-2 ubl domain, resonance broadening is observed in the presence of S5a. The hHR23a construct studied here contains the same 22 C-terminal residues, including a linker to a histidine tag, but this protein does not contain residues N-terminal to the ubl domain.

Figure 5B contains the chemical shift data for the hHR23a ubl domain plotted according to eq 1. These data are mapped onto the surface diagram of our modeled structure of the hHR23a ubl domain in Figure 6B to reveal that a surface in the hHR23a ubl domain very similar to that of the hPLIC-2 ubl domain binds S5a. The residues of hHR23a and hPLIC-2 at the S5a contact surface are largely identical. Furthermore, the S5a-binding surface of hHR23a is very similar geometrically and has an electrostatic potential similar to that of the hPLIC-2 ubl domain (Figure 6B).

The S5a-Binding Surface of the hPLIC-2 Ubl Domain Is Required for Proteasome Binding. To validate the identification of the S5a-binding surface on the hPLIC-2 ubl domain, we constructed a triple-amino acid substitution mutant in

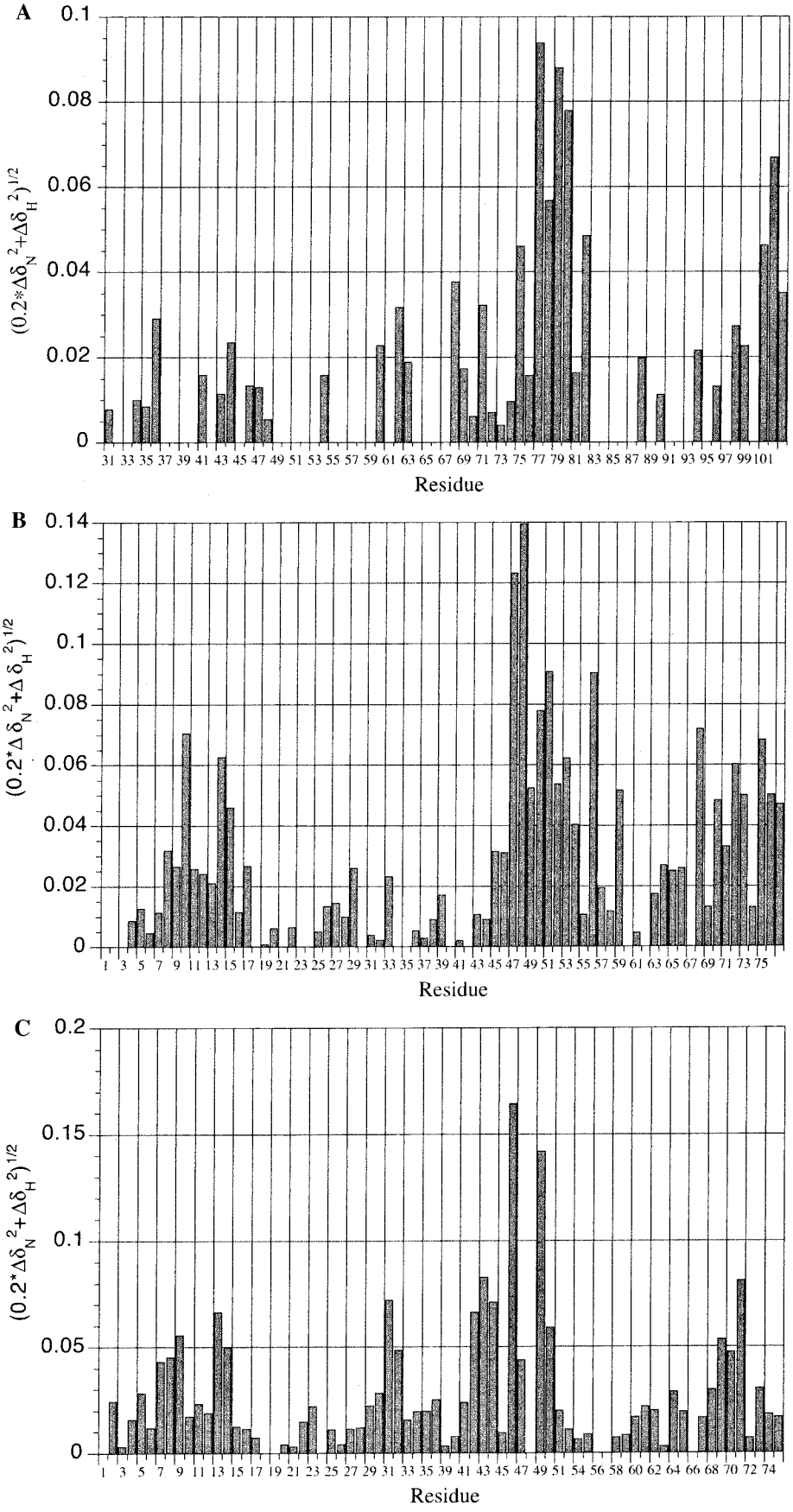

FIGURE 5: NMR chemical shift perturbation data for the hPLIC-2 ubl domain (A), the hHR23a ubl domain (B), and ubiquitin (C). These data are displayed for each residue according to equation 1 [$\sqrt{(0.2\delta_N^2)} + \delta_H^2$, where δ_N and δ_H represent the change in nitrogen and proton chemical shifts (in parts per million) upon S5a addition, respectively]. Residues that were excluded from this analysis include P40, P49, N51, and F57 of the hPLIC-2 ubl domain, P21, P42, and P60 of the hHR23a ubl domain, and K11, P19, P37, P38, and G53 of ubiquitin.

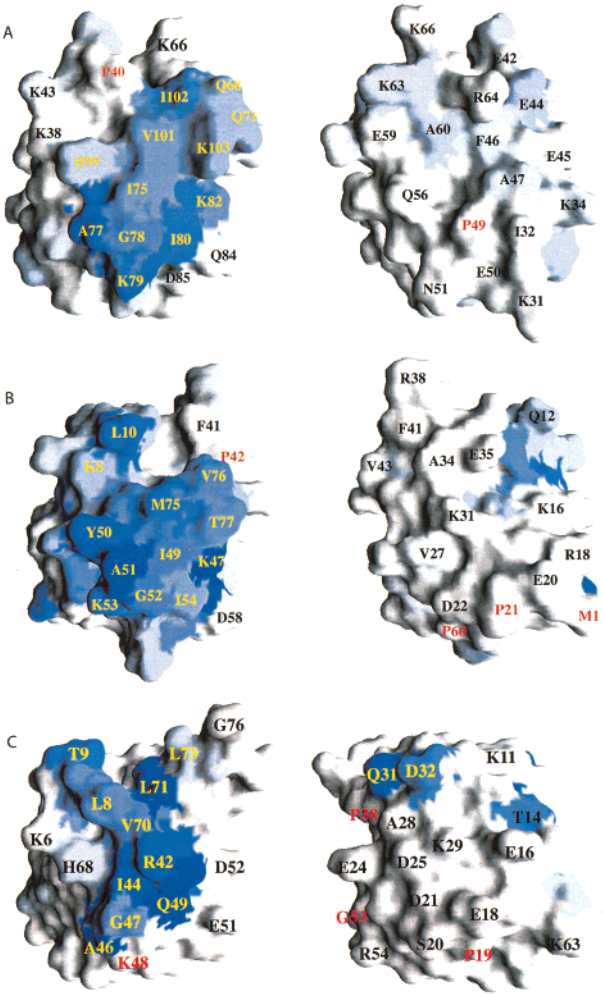

FIGURE 6: Mapping of the S5a-binding surface displayed in Figure 5 onto the surface diagrams of the ubl domains of hPLIC-2 (A) and hHR23a (B) and of ubiquitin (C). The orientation of the figures on the left is identical to that shown in Figures 2 and 3, whereas that on the right is rotated by 180°. A gradient based on the data displayed in Figure 5 was then built and plotted onto the surface diagrams such that the residues colored most blue experience the greatest chemical shift perturbation with S5a addition and those residues displayed in white are not perturbed by S5a addition. Those residues that could not be measured, including prolines, are labeled in red. This figure was produced by using GRASP (*51*).

which H99 and I75 were changed to alanine and A77 was changed to serine. The replacement of A77 with a serine residue produces a negative charge in the identified binding surface, and the replacement of H99 with an alanine removes the slightly positively charged histidine residue. A [^{1}H,^{15}N]-HSQC spectrum of the free triple mutant protein confirmed that the mutations did not cause any overall structural changes in the protein since chemical shift perturbations were observed only for the altered residues. A comparison of [^{1}H,^{15}N]HSQC spectra of the ^{15}N-labeled mutant alone with spectra for a 1:1 ubl domain:S5a molar ratio revealed that the mutant protein no longer specifically bound S5a (Figure 4C), thus confirming the ubl domain surface identified by NMR spectroscopy as the S5a contact surface. The amino acid substitutions in the mutated version of hPLIC-2 allow for weak nonspecific interaction with S5a, as the spectrum displayed in the right panel of Figure 4C contains cross-peaks that are slightly broadened relative to those in the [^{1}H,^{15}N]HSQC spectrum of the free mutant protein.

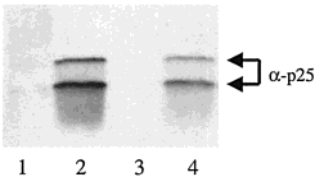

FIGURE 7: Western blot analysis of in vitro proteasomal binding of the hPLIC-2 wild-type and triple-mutant (I75A/A77S/H99A) ubl domain. Proteins from HeLa whole cell lysates bound to Ni−NTA beads with no overexpressed protein (lane 1), the wild-type ubl domain (lane 2), the triple-mutant ubl domain (lane 3), or a 50% mixture of the wild-type and triple-mutant ubl domains (lane 4) were analyzed as described in Materials and Methods using antibodies to the proteasome core subunit α-2.

Since it is possible that type 2 ubl domains could contact subunits other than S5a in the proteasome using different surfaces, we tested whether the hPLIC-2 ubl triple-substitution mutant could still bind to the proteasome using whole cell lysates from HeLa cells. Affinity-purified His-tagged wild-type and mutant hPLIC-2 ubl domains were tested for their ability to interact with proteasomes in whole cell lysates from HeLa cells by immunoblotting with α-p25, an antibody to the α-2 proteasomal core subunit (Figure 7). In these experiments, we found binding of the wild-type hPLIC-2 ubl domain to proteasomes, but not for the mutant ubl domain (Figure 7). We are able to conclude from these experiments that the surface conserved between the hPLIC-2 and hHR23a ubl domains that we have identified as required for S5a binding is also required for proteasome binding.

Residues on the Ubiquitin Surface Similar to the S5a-Binding Site of the Type 2 Ubl Domains Bind S5a. Competition experiments between monoubiquitin and polyubiquitin chains suggest that polyubiquitin chains preferentially bind S5a (*11*, *14*, *15*). To establish whether monoubiquitin binds S5a and whether such binding involves a surface similar to the hPLIC-2 ubl domain-binding surface, we performed titration experiments with ^{15}N-labeled ubiquitin and unlabeled S5a. Figure 4D depicts the [^{1}H,^{15}N]HSQC spectra of ^{15}N-labeled ubiquitin alone (left) and with a 1:1 ubl domain:S5a molar ratio (right). In the spectra for the 1:1 ubl domain:S5a molar ratio, fewer resonance cross-peaks originating from residues of ubiquitin disappear from a [^{1}H,^{15}N]HSQC spectrum than from those originating from the ubl type 2 domains at an identical molar ratio with S5a (Figure 4). The disappearance of residues is caused from the increased rotational correlation time of the larger bound state and from chemical exchange. The disappearance of all resonances except for the linker residues in the ubl domain of hPLIC-2 suggests that a tight complex has formed between the ubl domain of hPLIC-2 and S5a. In contrast, in the 1:1 complex with ubiquitin, only one residue completely disappears from the spectrum, indicating that the binding of ubiquitin to S5a is weaker than the binding of the ubl domain of hPLIC-2 with S5a.

Unlike the ubl domain of hHR23a, ubiquitin can bind to two different regions of S5a (*14*, *15*, *44*). If ubiquitin bound strongly to each of the two sites, one would expect that at a 2:1 ubiquitin:S5a molar ratio, the resonance signals of ubiquitin would be severely broadened as in the [^{1}H,^{15}N]-HSQC spectrum for the 1:1 hPLIC-2 ubl domain:S5a molar ratio. Our data suggest that ubiquitin complexes only weakly with S5a and dissociates easily. We continued these titration

experiments up to a molar ratio of one ubiquitin molecule to three S5a molecules. At that ratio, the signal intensity of the resonances originating from ubiquitin residues resembles that of the resonances originating from residues of the hPLIC-2 ubl domain when present at 1:1 ubl domain:S5a molar ratio (data not shown).

By using published resonance assignments (*45*, *46*), we measured the chemical shift perturbation of the ubiquitin amide nitrogen and proton atoms from the presence of S5a and have plotted the data according to eq 1 in Figure 5C. These data are mapped onto the surface diagram of ubiquitin to reveal a localized S5a-binding surface as shown in Figure 6C. Three residues (L8, I44, and V70) that have been previously identified by mutation studies as being important for ubiquitin binding the proteasome are included on this surface (*47*−*49*). The S5a-binding surface is not limited to these three residues, however, as contact with I44 and L70 would be structurally very difficult without contact with R42. We find that R42 and Q49 are definitely in the S5a contact surface in addition to other residues displayed in blue in Figure 6C. A comparison of Figures 3a and 6a with Figures 6a and 6c reveals that the surface on ubiquitin that we have identified as being required for binding S5a is more charged than the S5a contact surfaces of the hPLIC-2 and hHR23a ubl domain. The presence of charged and polar residues on this surface, including R42, Q49, and the nearby D52, may contribute to the weaker binding of ubiquitin to S5a compared with the binding of the hPLIC-2 and hHR23a ubl domain to S5a.

SUMO-1 Does Not Bind S5a. As mentioned above, the type 1 ubl protein SUMO-1 has a very different electrostatic surface than either ubiquitin or hPLIC-2 and hHR23a ubl domains. The surface in SUMO-1 similar to the S5a-binding surfaces that we have identified on the hPLIC-2 and hHR23a ubl domains and on ubiquitin is substantially more negatively charged in SUMO-1. On the basis of this observation, we expected that SUMO-1 would not bind S5a. To test this prediction, we performed titration experiments on ^{15}N-labeled SUMO-1 with unlabeled S5a. Figure 4E shows [^{1}H,^{15}N]-HSQC spectra of SUMO-1 alone and at a 1:1 SUMO-1:S5a molar ratio. Spectra acquired in the presence of S5a were unperturbed, confirming that SUMO-1 and S5a do not interact. Although SUMO-1 shares a fold very similar to that of the other proteins in this study, it has evolved very different surface properties presumably to perform different functions not directly involving proteolysis or binding to the proteasome. This study highlights the importance of characterizing the surface details of protein family members and reveals that subtle differences in electrostatic charge or hydrophobicity may underlie significant differences in function. More specifically, we are able to explain in this investigation why some proteins target the proteasome and others do not.

A Model of the Surface Diagram of the Segment in S5a That Binds Ubiquitin and the Type 2 Ubl Domains Reveals a Complementary Electrostatic Surface Potential. Two regions in S5a have previously been identified by deletion and site-directed mutation studies as being necessary for ubiquitin binding (*14*, *15*, *44*). The sequence of both of these regions in human (S5a) and yeast (Rpn10) is displayed in Figure 1B. The hydrophobic pattern of alternating long and short hydrophobic side chains is strictly required for binding

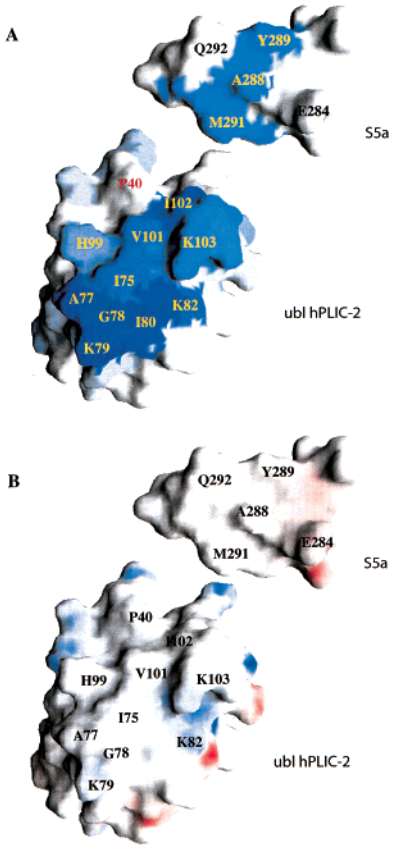

FIGURE 8: Model of how the ubl domain of hPLIC-2 and S5a may interact. The surface diagram on the left is of a model structure of the region of S5a required for binding the ubl domain of hHR23a. The surface diagram on the right is of the ubl domain of hPLIC-2. These structures are each oriented to expose the putative binding surfaces. In panel A, those residues of S5a reported to be critical for binding the hHR23a ubl domain are colored blue and those residues of the hPLIC-2 ubl domain that undergo chemical shift perturbations upon S5a addition are likewise colored blue as in Figure 5B. In panel B, the electrostatic surface potential of each molecule is mapped onto its surface diagram. This figure was produced using GRASP (*51*).

to each site. Secondary structure programs predict that each of these regions is helical. We built a model of the second ubiquitin-binding region reported to be critical for hHR23 ubl domain binding (*13*). On the basis of the high degree of similarity between the S5a contact surfaces of the ubl domains of hPLIC-2 and hHR23a, we presume that, like the ubl domain of hHR23a, the hPLIC-2 ubl domain would also only bind the second ubiquitin-binding site of S5a. Consequently, our model of the ubl domain-binding site of S5a includes residues S280−S294. We have built this model as an α-helix as predicted by secondary structure prediction programs and displayed a surface diagram of this element in Figure 8. We also display an hPLIC-2 ubl surface in Figure 8A identical to the left side of Figure 6A. It contains the data displayed in Figure 5A mapped onto a surface diagram of our calculated hPLIC-2 ubl structure. The S5a model displayed in Figure 8A is displayed with those residues of S5a that are reported from deletion studies to be critical for binding ubiquitin and the hHR23a domain colored blue (*13*). Inspection of the electrostatic surface potentials of the S5a peptide and the hPLIC-2 ubl domain mapped onto their respective surface diagrams, as displayed in Figure 8B, reveals these two molecules to be geometrically and elec-

trostatically complementary in their binding surfaces. Both molecules are largely hydrophobic in their binding region as indicated in white. Whereas the hydrophobic contact surfaces of both type 2 ubl domain proteins studied here and of ubiquitin are bound by basic residues (shown in blue), that of both ubiquitin-binding sites in S5a is bound by acidic residues (shown in red). The largely hydrophobic nature of the S5a residues that are critical for binding ubiquitin, italicized in Figure 1B, is most likely the origin of the weaker binding of the more charged ubiquitin molecule compared to the binding of the type 2 ubl domains studied here.

DISCUSSION

The Ubl Domains of hPLIC-2 and hHR23a Share a Highly Conserved Surface for Binding S5a. We have determined the structure of the ubl domain of hPLIC-2 and used this structure to generate a homology-based model of the ubl domain of hHR23a. The alignment used to generate this model was based on aligning the secondary structural elements of hPLIC-2 and hHR23a, which were determined by NMR spectroscopy (Figure 1A). The type 2 ubl domain of hPLIC-2 was found to more closely resemble ubiquitin than the type 1 ubl domain of SUMO-1. Each of the type 2 proteins binds S5a at a hydrophobic surface involving similar amino acids (Figure 6). The hydrophobic residues of the ubl domain of hPLIC-2 (A77, I75, I80, V101, and I102) correspond to A51, I49, I54, M75, and V76, respectively, of the hHR23a ubl domain. K82 in hPLIC-2 is also involved in binding S5a and occupies a position very similar to that of K47 in the hHR23a ubl domain. The S5a-binding surface was further confirmed by generating specific amino acid substitutions in the binding surface of the ubl domain of hPLIC-2 that abrogated binding to S5a (Figure 4C).

Ubiquitin Binds S5a More Weakly Than Do hPLIC-2 and hHR23a Ubl Domains through a Similar Hydrophobic Surface. Mammalian S5a contains two ubiquitin binding sequences with alternating long and short hydrophobic side chains (*14*, *15*, *44*). Although our studies do not allow us to distinguish between the binding of these segments by monoubiquitin, we found the surface on ubiquitin that binds S5a involves a surface similar to the S5a-binding surface of the type 2 ubl proteins. Although the two ubiquitin-binding segments in S5a share a similar sequence, since the structure of S5a has not yet been determined, we do not know yet if these segments differ in the context of the full protein.

The S5a interaction surface of ubiquitin that we have identified contains residues L8, V70, and I44, which had been reported from mutation studies of tetraubiquitin as being critical for binding to the proteasome (*47*−*49*). The S5a interaction surface, however, is not restricted to these residues. Charged and polar resides R42 and Q49 are also involved in binding S5a (Figures 5 and 6), and occupy positions corresponding to I75 and I80, respectively, in the hPLIC-2 ubl domain and to I49 and I54, respectively, in the hHR23a ubl domain. Furthermore, K82 in hPLIC-2 and K47 in hHR23a are replaced with D52 in ubiquitin. These amino acid differences provide an explanation for the weaker S5a binding that we observed for monoubiquitin than for either of the type 2 ubl domains that have been studied.

The electrostatic surface potential of the reported ubiquitin- or ubl-binding region of S5a reveals a predominantly hydrophobic surface with surrounding acidic residues (Figure 8). The electrostatic potential of this surface is complementary to the electrostatic potential of the surfaces used by ubiquitin and the type 2 ubl domains to bind S5a. The surfaces within these proteins implicated in binding S5a are predominately hydrophobic with surrounding basic residues.

Interestingly, SUMO-1 shares a similar fold with the type 2 ubiquitin-like proteins and ubiquitin, but differs in its electrostatic surface potential and does not bind S5a (Figure 4E). The ubiquitin structural motif shared by many proteins has therefore evolved different electrostatic surfaces to perform distinct functions. Our comparison of the various members of the ubiquitin family proteins highlights the importance of using protein surfaces for functional predictions and correlations, rather than protein folds.

The Identified S5a-Binding Surface Is Required for General Proteasome Binding. The second ubiquitin-binding site of S5 is required for hHR23 binding (*13*−*15*, *44*). As shown in Figure 1B, the yeast homologue of S5a, Rpn10, is shorter and lacks this second ubiquitin-binding site (PubS2). S5a is the only proteasome subunit that has been identified to directly bind ubiquitin or hHR23. Yet yeast strains lacking the gene homologue Rpn10 exhibit only minor growth defects, suggesting that other subunits of the proteasome may contribute to polyubiquitin chain recognition (*18*, *19*). We suspect that the type 2 ubl domains of hPLIC-2 and hHR23a may not bind the yeast Rpn10 since it lacks PubS2. The role of the yeast homologues of hHR23a and hPLIC-2 in degradation may be very different from the roles of the mammalian counterpart. Nevertheless, we tested whether the S5a-binding surface that we identified in these type 2 ubl domains was required for proteasome binding. We found that the specific amino acid substitutions within the S5a-binding surface of the hPLIC-2 ubl domain that abrogated binding to S5a also abrogated binding to the proteasome. This result provides the first evidence that the S5a-binding surface of the hPLIC-2 ubl domain is required for proteasome binding. We do not exclude the possibility, however, that this same surface might be binding other proteasome subunits.

Understanding the mechanisms by which proteins are recruited to the proteasome for degradation could be important for designing specific inhibitors of proteasome-dependent proteolysis. In summary, we have determined the solution structure of the type 2 ubl domain of hPLIC-2. We have used this structure in combination with NMR data providing secondary structure information for generating a model structure of the ubl domain of hHR23a. We have found that these two proteins share a highly conserved surface in their ubl domains that is important for S5a and proteasome binding. This surface is modified in ubiquitin, accounting for the weaker binding of ubiquitin to S5a that we observe. The analogous surface on SUMO-1 has dramatically altered electrostatic properties, and SUMO-1 did not bind S5a. In this work, we have elucidated the proteasome-binding surface of the ubiquitin family of proteins and have provided an example of proteins with similar folds that have evolved different surfaces to perform different functions. This study highlights the importance of studying protein surfaces, rather than protein folds, for function predictions.

ACKNOWLEDGMENT

We are grateful to Dr. Fumio Hanaoka for providing the S5a plasmid used in this study. We gratefully acknowledge Stephen J. Simmons for his assistance with protein expression and purification and Greg Heffron for technical assistance with the NMR spectrometers. We are also grateful to Dr. James Chou and Dr. Ad Bax for sending us their ubiquitin chemical shift assignments.

SUPPORTING INFORMATION AVAILABLE

Enlarged view of a portion of the spectra shown in Figure 4. This material is available free of charge via the Internet at http://pubs.acs.org.

REFERENCES

1. Baumeister, W., Walz, J., Zuhl, F., and Seemuller, E. (1998) *Cell 92*, 367−380.
2. Coux, O., Tanaka, K., and Goldberg, A. L. (1996) *Annu. Rev. Biochem. 65*, 801−847.
3. Hilt, W., and Wolf, D. H. (1996) *Trends Biochem. Sci. 21*, 96−102.
4. Goldberg, A. L., Gaczynska, M., Grant, E., Michalek, M., and Rock, K. L. (1995) *Cold Spring Harbor Symp. Quant. Biol. 60*, 479−490.
5. Heemels, M. T., and Ploegh, H. (1995) *Annu. Rev. Biochem. 64*, 463−491.
6. Ciechanover, A. (1998) *EMBO J. 17*, 7151−7160.
7. Ciechanover, A. (1994) *Cell 79*, 13−21.
8. Hochstrasser, M. (1996) *Annu. Rev. Genet. 30*, 405−439.
9. Vierstra, R. D. (1996) *Plant Mol. Biol. 32*, 275−302.
10. Voges, D., Zwickl, P., and Baumeister, W. (1999) *Annu. Rev. Biochem. 68*, 1015−1068.
11. Deveraux, Q., Ustrell, V., Pickart, C., and Rechsteiner, M. (1994) *J. Biol. Chem. 269*, 7059−7061.
12. Ferrell, K., Deveraux, Q., van Nocker, S., and Rechsteiner, M. (1996) *FEBS Lett. 381*, 143−148.
13. Hiyama, H., Yokoi, M., Masutani, C., Sugasawa, K., Maekawa, T., Tanaka, K., Hoeijmakers, J. H., and Hanaoka, F. (1999) *J. Biol. Chem. 274*, 28019−28025.
14. Young, P., Deveraux, Q., Beal, R. E., Pickart, C. M., and Rechsteiner, M. (1998) *J. Biol. Chem. 273*, 5461−5467.
15. Haracska, L., and Udvardy, A. (1997) *FEBS Lett. 412*, 331−336.
16. Ghislain, M., Udvardy, A., and Mann, C. (1993) *Nature 366*, 358−362.
17. Gordon, C., McGurk, G., Dillon, P., Rosen, C., and Hastie, N. D. (1993) *Nature 366*, 355−357.
18. van Nocker, S., Sadis, S., Rubin, D. M., Glickman, M., Fu, H., Coux, O., Wefes, I., Finley, D., and Vierstra, R. D. (1996) *Mol. Cell. Biol. 16*, 6020−6028.
19. Kominami, K., Okura, N., Kawamura, M., DeMartino, G. N., Slaughter, C. A., Shimbara, N., Chung, C. H., Fujimuro, M., Yokosawa, H., Shimizu, Y., Tanahashi, N., Tanaka, K., and Toh-e, A. (1997) *Mol. Biol. Cell 8*, 171−187.
20. Lambertson, D., Chen, L., and Madura, K. (1999) *Genetics 153*, 69−79.
21. Jentsch, S., and Pyrowolakis, G. (2000) *Trends Cell Biol. 10*, 335−342.
22. Melchior, F. (2000) *Annu. Rev. Cell Dev. Biol. 16*, 591−626.
23. Biggins, S., Ivanovska, I., and Rose, M. D. (1996) *J. Cell Biol. 133*, 1331−1346.
24. Miller, R. D., Prakash, L., and Prakash, S. (1982) *Mol. Gen. Genet. 188*, 235−239.
25. Wang, Z., Wei, S., Reed, S. H., Wu, X., Svejstrup, J. Q., Feaver, W. J., Kornberg, R. D., and Friedberg, E. C. (1997) *Mol. Cell. Biol. 17*, 635−643.
26. Masutani, C., Sugasawa, K., Yanagisawa, J., Sonoyama, T., Ui, M., Enomoto, T., Takio, K., Tanaka, K., van der Spek, P. J., Bootsma, D., et al. (1994) *EMBO J. 13*, 1831−1843.
27. Wu, A. L., Wang, J., Zheleznyak, A., and Brown, E. J. (1999) *Mol. Cell 4*, 619−625.
28. Kleijnen, M. F., Shih, A. H., Zhou, P., Kumar, S., Soccio, R. E., Kedersha, N. L., Gill, G., and Howley, P. M. (2000) *Mol. Cell 6*, 409−419.
29. Kumar, S., Talis, A. L., and Howley, P. M. (1999) *J. Biol. Chem. 274*, 18785−18792.
30. Grzesiek, S., and Bax, A. (1992) *J. Magn. Reson. 96*, 432−440.
31. Wishart, D. S., Sykes, B. D., and Richards, F. M. (1991) *J. Mol. Biol. 222*, 311−333.
32. Wishart, D. S., Sykes, B. D., and Richards, F. M. (1992) *Biochemistry 31*, 1647−1651.
33. Wüthrich, K. (1986) *NMR of Proteins and Nucleic Acids*, Wiley, New York.
34. Bartels, C., Xia, T.-H., Billeter, M., Güntert, P., and Wüthrich, K. (1995) *J. Biomol. NMR 6*, 1−10.
35. Cornilescu, G., Delaglio, F., and Bax, A. (1999) *J. Biomol. NMR 13*, 289−302.
36. Nilges, M., Clore, G. M., and Gronenborn, A. M. (1988) *FEBS Lett. 239*, 129−136.
37. Brünger, A. T. (1993) *XPLOR Version 3.1: A System for X-ray Crystallography and NMR*, Yale University Press, New Haven, CT.
38. Walters, K. J., Gassner, G. T., Lippard, S. J., and Wagner, G. (1999) *Proc. Natl. Acad. Sci. U.S.A. 96*, 7877−7882.
39. Vijay-Kumar, S., Bugg, C. E., Wilkinson, K. D., and Cook, W. J. (1985) *Proc. Natl. Acad. Sci. U.S.A. 82*, 3582−3585.
40. Vijay-Kumar, S., Bugg, C. E., and Cook, W. J. (1987) *J. Mol. Biol. 194*, 531−544.
41. Bayer, P., Arndt, A., Metzger, S., Mahajan, R., Melchior, F., Jaenicke, R., and Becker, J. (1998) *J. Mol. Biol. 280*, 275−286.
42. Cavanagh, J., Fairbrother, W. J., Palmer, A. G., III, and Skelton, N. J. (1996) *Protein NMR Spectroscopy Principles and Practice*, Academic Press, San Diego.
43. Levitt, M. (1995) *Look, version 2.0*, Molecular Application Group, Stanford University and Yeda.
44. Fu, H., Sadis, S., Rubin, D. M., Glickman, M., van Nocker, S., Finley, D., and Vierstra, R. D. (1998) *J. Biol. Chem. 273*, 1970−1981.
45. Weber, P. L., Brown, S. C., and Mueller, L. (1987) *Biochemistry 26*, 7282−7290.
46. Cornilescu, G., Marquardt, J. L., Ottiger, M., and Bax, A. (1998) *J. Am. Chem. Soc. 120*, 6836−6837.
47. Beal, R., Deveraux, Q., Xia, G., Rechsteiner, M., and Pickart, C. (1996) *Proc. Natl. Acad. Sci. U.S.A. 93*, 861−866.
48. Beal, R. E., Toscano-Cantaffa, D., Young, P., Rechsteiner, M., and Pickart, C. M. (1998) *Biochemistry 37*, 2925−2934.
49. Thrower, J. S., Hoffman, L., Rechsteiner, M., and Pickart, C. M. (2000) *EMBO J. 19*, 94−102.
50. Koradi, R., Billeter, M., and Wüthrich, K. (1996) *J. Mol. Graphics 14*, 51−55.
51. Nicholls, A. J. (1993) *GRASP Manual*, Columbia University, New York.

BI011892Y